The attitude of the vehicle was pitch 0°, yaw 180°, and roll −10°. That is, the orbiter was flying with the bay pointing away from the earth, the tail forward, and the port wing tilted down 10° so that the limb was in the AEPI field of view. The attitude was selected so that the AEPI instrument could make these earth limb observations.

A ground support software routine devised before the mission allowed the computation of the earth's magnetic field lines in the vicinity of the orbiter. The computer was tied into an image memory so that the position of the calculated field lines could be displayed on a TV monitor. This enabled us to display the apparent position of a set of magnetic field lines in the vicinity of the orbiter. Figure 1B shows the computed field line plots corresponding to the AEPI television field of view 5 minutes before, during, and 5 minutes after the observation of the equatorial magnesium ions. For each set, five field lines were plotted. The first field line was selected to go through a point located on the line of sight corresponding to the center of the picture, that is, located on the system's optic axis. This point is at a distance D in front of the optical system. For Fig. 1B, D was 1400 km, which gave the best match between the shape of magnetic field line and the observed Mg^+ fingers. For each set, the central field lines go through this point. The field lines were plotted as points at every 10 km from 100 km altitude up. This technique was used to illustrate the foreshortening of the field lines due to perspective effects. Besides the central field line, the four adjacent field lines in a set were selected by a fixed geographic latitude and longitude offset corresponding to a four-point square grid around the central field line.

Thus we can see that the observed magnesium striations are parallel to the magnetic field line located 1400 km from the orbiter. The selection of the field line defines the altitude of the center point of the image, which is 180 km for this case.

From these AEPI observations, it can be seen that imaging of the earth's ionosphere through the presence of the natural Mg^+ tracer ions is feasible. Quantitative analysis of this event and many other observations is in progress.

The hand-held image-intensifier camera permitted the observation of atmospheric airglow and of the glow associated with the shuttle. This camera could be operated in white light, in a filtered mode, or in a dispersion mode. In the dispersion mode, a diffraction grating was placed in front of the lens and the image produced was a result of diffraction through this objective grating.

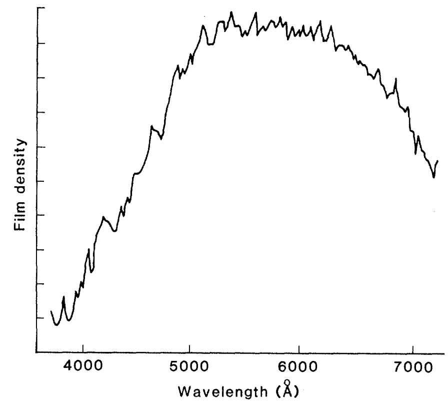

Fig. 3. Microdensitometer tracing of an image of spacecraft glow showing a structureless red glow.

The airglow spectrum in Fig. 2A shows a zero-order image of the earth's airglow layer on the left and first-order dispersion on the right. Note that the spacecraft orbital maneuvering system (OMS) pod indicates the airglow source at the lower right. The first spectral feature is a 5577-Å emission from atomic oxygen and the brightest feature is at 7620 Å. The 7620-Å feature was previously identified (*2*) as being the O_2 atmospheric bands. Figure 2B shows a microdensitometer tracing of the spectrum of Fig. 2A; the OH components were obtained from a 200-Å synthetic spectrum of vibrational transitions of OH (*8*).

A ram glow has been reported from earlier observations associated with the Atmospheric Explorer and Dynamic Explorer spacecraft (*9, 10*). The spatial distribution of the glow was observed from the orbiter vertical stabilizer as well as the OMS pod (*3*). Shown in Fig. 3 is a microdensitometer tracing of the spectrum of the spacecraft glow on the vertical stabilizer. Note that this tracing shows none of the structure that was seen in the airglow spectrum of Fig. 2B. It was suggested earlier (*11*) that OH might be a candidate species for producing the glow; however, it does not appear that OH plays a dominant part in the process resulting in the glow emission on the orbiter stabilizer.

The hand-held image intensifier camera was used to make many observations of the natural limb airglow layer. Because of the favorable transmission characteristics of the Spacelab view ports, the spectral observing regions could be extended farther toward the infrared. The naturally occurring OH Meinel bands were photographed in the airglow but were absent in similar photographs of the spacecraft glow. We are currently making a quantitative analysis of these types of images.

S. B. MENDE

Lockheed Palo Alto Research Laboratory, Palo Alto, California 94304

G. R. SWENSON

K. S. CLIFTON

Space Science Laboratory, NASA–Marshall Space Flight Center, Huntsville, Alabama 35812

References and Notes

1. W. G. Sandie, S. B. Mende, G. R. Swenson, M. E. Polites, *Opt. Eng.* **22**, 756 (1983).
2. S. B. Mende, P. M. Banks, R. Nobles, O. K. Garriott, J. Hoffman, *Geophys. Res. Lett.* **10**, 1108 (1983).
3. ——, *J. Spacecr. Rockets*, in press.
4. S. B. Mende, P. M. Banks, Da. A. Klingelsmith III, *Geophys. Res. Lett.* **11**, 527 (1984).
5. A. Boksenberg and J. C. Gerard, *J. Geophys. Res.* **76**, 4641 (1973).
6. J. C. Gerard, *ibid.*, **81**, 83 (1976).
7. —— and A. Monfils, *ibid.* **83**, 4389 (1978).
8. S. Langhoff, personal communication.
9. J. H. Yee and V. J. Abreu, *Geophys. Res. Lett.* **10**, 126 (1983).
10. V. J. Abreu, W. R. Skinner, P. B. Hays, J. H. Yee, in *Proceedings of the AIAA Shuttle Environment and Operations Meeting* (AIAA, New York, 1983), p. 178.
11. T. G. Slanger, *Geophys. Res. Lett.* **10**, 130 (1983).
12. The flight of AEPI on Spacelab 1 was the result of the dedicated efforts of many people. We express our gratitude to all those at Lockheed Missile and Space Company and at Marshall Space Flight Center who were involved in the design and development of the AEPI instrument. We are also indebted to those who were involved in the integration and flight operations of Spacelab 1 at Marshall, Kennedy, and Johnson space centers. Special thanks are due to the crew of STS-9. The work at Lockheed was supported by NASA under contract NAS 8-32579.

27 March 1984; accepted 10 May 1984

Isotopic Stack: Measurement of Heavy Cosmic Rays

Abstract. *A stack of plastic nuclear track detectors was exposed to heavy cosmic rays on the pallet of Spacelab 1. Some layers of the stack were rotated with respect to the main stack to determine the arrival time of the particles. After return of the stack the latent particle tracks are revealed by chemical etching. Under the optical microscope the charge, mass, energy, and impact direction of the particles can be deduced from the track geometry.*

Experiment objectives. Experiment 1ES024 on Spacelab 1 was designed to measure the chemical composition and energy spectra of heavy cosmic-ray nuclei with nuclear charge equal to or greater than 3. The exposure of a stack of nuclear track detectors on the Spacelab pallet allows the study of different particle components in the energy range 20 to 700 MeV per nucleon. At higher energies the isotopic composition of the galactic cosmic rays can be analyzed, giving information on the source, acceleration, and propagation of these particles, which originated in distant stars and have traversed the universe for millions of years. Below 100 MeV per nucleon, particles from the radiation belt and the anomalous component can be detected. The actual number of particles collected depends on the altitude and inclination of the shuttle orbit and on the shuttle attitudes and the solar activity during the mission.

The impact time of most of the particles can be correlated with the orbit position of the shuttle and thus with geomagnetic field parameters. By calculating the inverse motion of these particles we can study "geomagnetically forbidden" particles and estimate ionization states for the required rigidity. Figure 1 shows an example of a calculated trajectory in the geomagnetic field for a high-energy cosmic-ray particle.

Table 1. Approximate values of cutoff rigidity (R) and kinetic energy (E_{kin}) for M/Z = 2 as a function of L-shell values at vertical incidence. R_E = earth radii.

L (R_E)	R (GV)	E_{kin} (MeV per nucleon)
2.5	2.54	600
3.2	1.55	280
4.0	0.98	100
5.0	0.63	40
6.0	0.44	20

Experiment design. The apparatus consists of a stack of nuclear track detectors. The experiment aperture is 1480 cm^2 with an almost 2π-steradian field of view; the depth is 7.9 g/cm^2. The main stack consists of 140 foils of 0.3-mm-thick carbonate CR-39, and has a total thickness of 43.2 mm. Besides this main detector material, one layer of cellulose nitrate and one of polycarbonate are used on the top and a stack of polycarbonate foils is used at the bottom. Above the material at the top is a thermal shield, which consits of Kapton and Tedlar foils. A part of the stack consisting of eight CR-39 sheets is rotated one revolution during the mission. The corresponding track segments in the fixed and rotated stack can be aligned after recovery and thus the arrival time of the individual particle can be deduced.

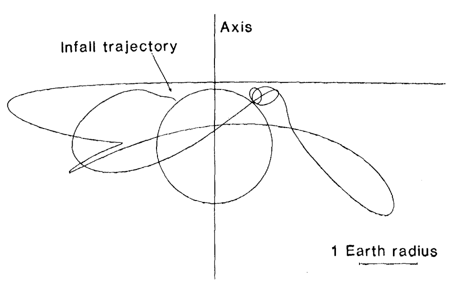

Fig. 1. Particle trajectory for an ion of mass-to-charge ratio M/Z = 2 ion with a rigidity of 4.03 GV in the geomagnetic field (vertically incident at 50°N, 60°E and 250 km altitude).

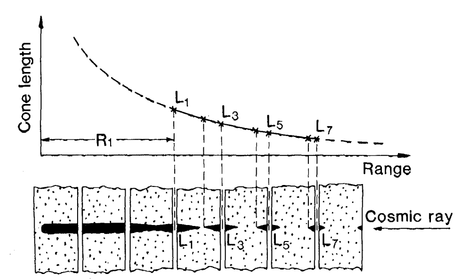

Fig. 2. Image of a stopping heavy-ion track in plastic detectors with a plot of the cone length versus residual range dependence (track image not to scale).

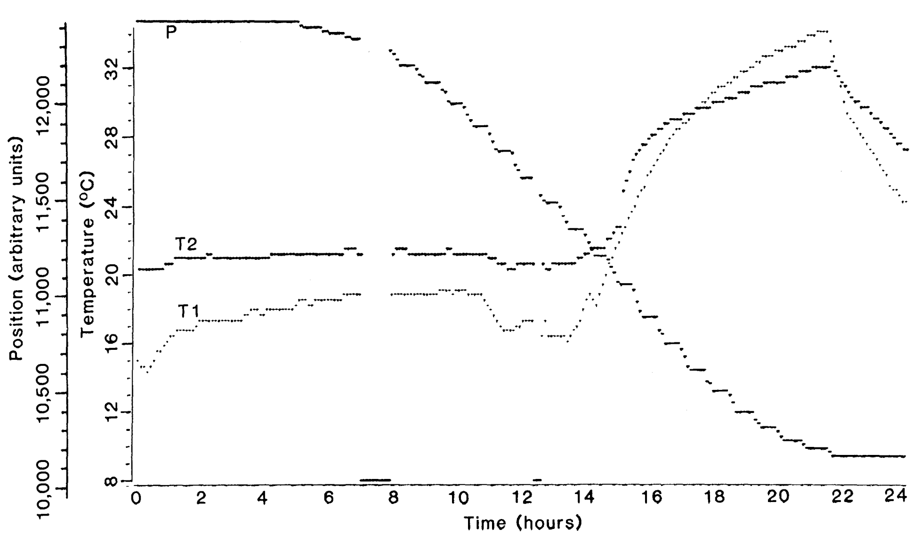

Fig. 3. Position encoder output (P) and temperature ($T1$ and $T2$) history from 6:12:00:00 to 7:12:00:00 MET. Two gaps in the data transmission can be seen.

Heavy ions stopping in or passing through the plastic sheets of the stack produce latent tracks, which can be revealed by chemical etching in the laboratory. Further analysis can be done under optical and electron microscopes by measuring the shape and length of the etched cones (Fig. 2). These parameters strongly depend on the energy loss along the trajectory of the incoming particle (*1*).

Mission operation. The experiment was powered at 0:12:00:00 mission elapsed time (MET) and operated nominally until 7:21:30:00 MET, when the rotation was terminated after one complete revolution. Step commands for the stack movement were automatically generated by the onboard command and data management system (CDMS). Orbit position data from the shuttle were fed to the CDMS and the corresponding McIlwain parameter values, L, were calculated from a simple dipolar magnetic field model. An accurate L-parameter history (L as a function of MET) was provided by NASA (*2*). When one of the threshold values in Table 1 was crossed (with an increasing or decreasing tendency), a step command was sent by the CDMS and the rotating stack moved about 0.37°. The absolute position of the rotating stack was monitored by a 13-bit angular encoder with 0.0226° resolution, sampled once per second, and transmitted together with temperature data from the top and bottom of the stack via the tracking/data relay satellite to the ground.

The stepping frequency depended mainly on the correlation between the orbital plane and the magnetic axis. The highest stepping rate occurred when high geographic latitudes were reached close to the magnetic poles under minimum geomagnetic cutoff. Figure 3 shows the temperature and stepping history from 6:12:00:00 to 7:12:00:00 MET with the significant temperature rise during the first hot test.

Quick-look results. The experiment performed nominally and returned in good shape. The scientific data are stored in latent tracks. Some sheets of the stack were etched and scanned. Tracks of cosmic rays were identified as well as tracks of ^{56}Fe ions with an energy of 410 MeV per nucleon from the post-flight calibration of the detector foils, which was performed at Lawrence Berkeley Laboratory.

R. BEAUJEAN, M. SCHMIDT, W. ENGE
G. SIEGMON, J. KRAUSE, E. FISCHER
Institut für Reine und Angewandte Kernphysik, Universität Kiel, 2300 Kiel, Federal Republic of Germany

References and Notes

1. R. Beaujean and W. Enge, *Nucl. Track Detect.* **1**, 19 (1977).
2. *Spacelab 1 Flight Definition Document, JA-024* (NASA-Marshall Space Flight Center, Huntsville, Ala., June 1983).
3. We thank Professor Wibberenz for his support and the staff of the Lawrence Berkeley Laboratory for irradiation of the detector foils. The financial support of the federal government (BMFT) is acknowledged.

27 March 1984; accepted 30 May 1984

Space Experiments with Particle Accelerators

Abstract. *Electron and plasma beams and neutral gas plumes were injected into the space environment by instruments on Spacelab 1, and various diagnostic measurements including television camera observations were performed. The results yield information on vehicle charging and neutralization, beam-plasma interactions, and ionization enhancement by neutral beam injection.*

Space experiments with particle accelerators (SEPAC) constituted experiment 1NS002 on Spacelab 1. The program included active and interactive experiments on and in the earth's upper atmosphere and magnetosphere. The purpose was to gain insight into the physical processes that take place in the envelope of magnetic fields and charged particles surrounding the earth as well as in magnetic environments elsewhere in the universe (*1, 2*). Significant results were obtained on (i) vehicle charging and neutralization effects, (ii) beam-plasma interactions associated with electron beam emissions, and (iii) ionization enhancement by neutral beam injection.

The SEPAC experiments involved injection of electron and plasma beams and neutral gas clouds into the space environment. This was accomplished with an electron beam accelerator (EBA), operating at 7.5 kV with a maximum current of 1.6 A and a pulse duration of 10 to 5000 msec, a magneto-plasma dynamic (MPD) arcjet, which injected Ar gas at 2 kJ per 1-msec pulse, and a neutral gas plume injector, which injected N_2 gas at 10^{23} molecules per 100-msec pulse. In addition, the instrumentation included a monitor television camera (low-light-level TV), a diagnostic package consisting of a photometer and particle and wave probes, and control and display hardware consisting of an interface unit, dedicated experiment processor, and control panel.

Before the various scientific experiments were carried out, an instrument performance test and MPD and EBA beam-firing tests were performed. The instruments and their operational capabilities were tested successfully. After this initial feasibility test was completed several scientific functional objectives were followed. However, a malfunction of the EBA occurred later in the mission, and operation of high-power modes of the EBA was not possible. Consequently, the SEPAC experiments thereafter were performed with the MPD arcjet, neutral gas plume, diagnostic package, and monitor TV only.

Vehicle charge buildup and neutralization. It was observed that when the EBA was operated at a power level above approximately 100 W the payload bay was so brightly illuminated by the bombarding return electrons that a definite beam shape was difficult to observe. The glow occupied a broad area above the EBA accelerator, suggesting that a glow discharge took place in the vicinity of the spacecraft. The charge buildup on the vehicle body due to EBA electron beam emissions was quantitatively determined by means of a Langmuir probe, a floating charge probe, and a particle energy analyzer. The particle energy analyzer monitored the energy spectrum of returning electrons, the peak in the energy spectrum being used to estimate the electrical potential due to vehicle charge buildup. In the very-low-power mode of EBA operation, the charging potential is proportional to the EBA beam current. As shown in Fig. 1, however, at an EBA current above 100 mA, the vehicle charge potential sometimes shows a saturation effect, giving a value equal to the beam energy. The spread of vehicle potential is due to the different attitudes of the spacecraft and the variety of ionospheric conditions.

An attempt to neutralize vehicle charge buildup was made by injecting an

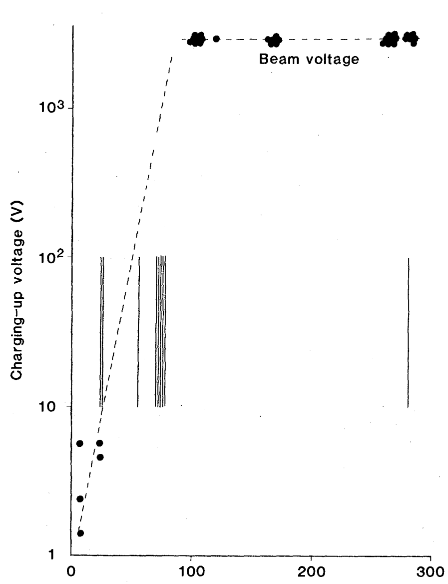

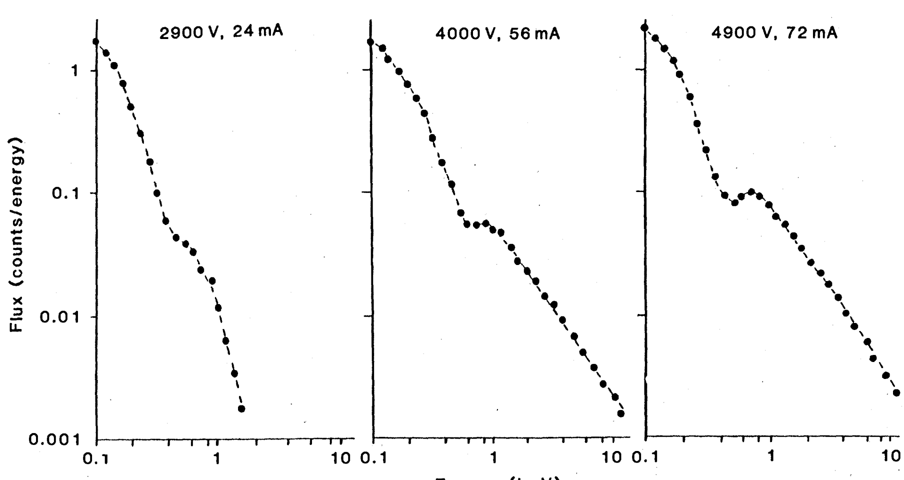

Fig. 1 (left). Vehicle charging-up potential plotted against electron beam current. Closed circles include data from the Langmuir probe, the floating charge probe, and the particle energy analyzer. Vertical lines indicate probable values, which are not determined without ambiguity. Fig. 2 (right). Energy spectrum of returning electrons measured by the particle energy analyzer.